A 32-Channel Fully-Digital Adaptive Applebaum Aperture at 5.8 GHz for Array RF Sensing

Umesha Kumarasiri, Sivakumar Sivasankar, Chamira Edussooriya*, Viduneth Ariyarathna and Arjuna Madanayake†
Florida International University, Miami, FL, USA
*University of Moratuwa, Moratuwa, Sri Lanka
Emails: †amadanay@fiu.edu

***Abstract*—The real-time adaptive nulling of a digital beamformer is crucial for receiving weak signals in a high RFI or RF denied environment. The Howells-Applebaum and MVDR adaptive beamformers use the Weiner optimum solution to ensure that RFI sources are blanked out in an array processor. In this paper, we create a custom 32-channel fully-digital array operating at 5.7-5.8 GHz, with real-time FPGA processing for both adaptation and subsequent beamforming with RFI suppression. Real-time measurements with up to three RFI sources show correct real-time digital beamforming in the FPGA processor. The developed microwave and digital systems along with hardware accelerated Howells-Applebaum array-null adaptation architecture will be used as a building block to create RF identification, location, spectrum sensing, and wireless communications that are resilient to jammers and RFI sources in the environment.**

***Index Terms*—Adaptive beamformer, FPGA, digital, arrays.**

I. Introduction

The radio frequency (RF) spectrum is the invisible combat zone in modern warfare. The warfighter's life depends on command and control of the electromagnetic spectrum under highly contested, congested, and denied environments. The modern theatre is an extremely dangerous place owing to the silent and invisible threat that is electronic warfare (EW). Technologies such as cyberattacks may target wireless communication systems, location and RF indentification (ID) techologies, and sensors such as radars using manipulative tactics on the RF spectrum. Drones pose a massive RF jamming threat as the enemy may be able to deploy hundreds if not thousands of RF jammers scattered across the sky making precision sensing or communications extremely difficult.

For example, imagine a scenario where an active electronically scanned aperture (AESA) is operating as a multifunctional communications and radar sensor in an environment where there as a hundred micro unmanned aerial systems (mUAS) each fitted with a 1 W power jammer. This jammer cloud can operate at relatively close range to the AESA (at 1 km range, say) making it extremely difficult for the sensitive receivers to detect faint signals from far-away targets (say 200 km) as the jammer cloud would simply dwarf the signals of interest. The conventional EW situation where a single high power jammer pod on an enemy aircraft has been replaced by hundreds of low power jammers aboard mUAS swarm. Thankfully, battery life constraints aboard the mUAS limit the individual transmit powers to be quite low, where by "low" we mean not in the kilo watt range. When deployed at scale of thousands, we guesstimate that the RF jammer transmit power per drone would probably be less than about 30 dBm; this is quite sufficient to completely blind a sensitive AESA sensor at ranges of few kms.

The important point is that although received jammer power levels expected at the AESA would be enough to prevent its operation, unlike a kilo watt or megawatt class jammer which may completely saturate the RF front-ends, low powered jammers can be more or less removed using carefully designed digital signal processor (DSP) algorithms because the level of over-drive at the AESA receivers may not be severe enough to prevent any DSP operations. In other words, they are not driven into clip and jammer powers are within about 50 dB of the signals of interest. A typical high-performance AESA may use about 16 bits of precision in the data convertors; allowing 8 bits for jammer dynamic range (about 50 dB) we are still left with about 8 bits for the signal of interest, which is probably sufficient for many signal processing, optimal detection and machine learning (ML) algorithms to detect a radar signature or communication signal. The most important point is that if the jammer signals are excessive in its power level, DSP may remove the jammers but the residual signal of interest may not have the resolution required for the level of resilience needed in the application.

While noting these constraints, we describe our university research on the design, implementation and test of fully-digital adaptive aperture algorithms employing state of the art (SOTA) adaptive nulling using the well-known Weiner optimum weight vector. Our algorithm of choice is a fully digital realization of the Howells-Applebaum adaptive beamformer which is perfect for sensing as it allows the main beam (primary lobe of the array pattern) to be pointed to the desired direction while the nulls are learned from measurements of the RF environment.

II. Review of Optimum Beamforming

We briefly review two statistically optimum beamformers. Consider a uniform linear array (ULA) of N antennas. The ULA receives a signal of interest having a direction of arrival (DOA) $\theta_0 \in [-90^\circ, 90^\circ]$ and multiple (less than

This effort was sponsored in whole or in part by the United States National Science Foundation (NSF).

$N-1$) radio frequency interference (RFI) waves having DOAs different to θ_0. We assume that both signal of interest and RFI are widesense stationary (WSS) narrowband plane waves. The signals received by a ULA are received via RF chains consisting of low-noise amplifiers (LNAs), filters and mixers before synchronous analog-to-digital conversion (ADC). We denote the input signal to the beamformer at a time instant as $\boldsymbol{x} = [x(0), x(1), \ldots, x(N-1)]^{\mathrm{T}}$, where $x(k)$, $0 \leq k \leq (N-1)$ is the discrete-time signal corresponding to the kth element. We denote the weight vector of a beamformer as $\boldsymbol{w} = [w(0), w(1), \ldots, w(N-1)]^{\mathrm{T}}$. Note that $\boldsymbol{x}, \boldsymbol{w} \in \mathbb{C}^N$.

A. Howells-Applebaum Beamformer

In the Howells-Applebaum beamformer [1], [2], the weights are selected to maximize the signal-to-noise ratio (SNR). The optimal weight vector $\boldsymbol{w}$ is

$$\boldsymbol{w} = \boldsymbol{R}^{-1}\boldsymbol{a}, \tag{1}$$

where $\boldsymbol{R} = \mathbb{E}\{\boldsymbol{x}\boldsymbol{x}^{\mathrm{H}}\}$ ($\in \mathbb{C}^{N\times N}$) is the covariance matrix, and $\mathbb{E}\{\cdot\}$ and $(\cdot)^H$ denote the expectation and Hermitian (conjugate transpose) of a matrix, respectively. Furthermore, $\boldsymbol{a} = [1, e^{j\tau}, \ldots, e^{j(N-1)\tau}]^{\mathrm{T}} \in \mathbb{C}^N$ is the steering vector, and $\tau = 2\pi d \sin(\theta_0)/\lambda$, where d is the inter-antenna distance and λ is the wavelength of the narrowband plane wave. In practice, $\boldsymbol{R}$ is estimated using a set of temporal samples (snapshots) because the signals represent WSS processes. The output y of the beamformer is given by $y = \boldsymbol{w}^{\mathrm{H}}\boldsymbol{x}$.

B. MVDR Beamformer

The minimum variance distortionless response (MVDR) beamformer minimizes the power of the received signal while constraining the array response at θ_0 to a desired value. Weights of the MVDR beamformer is the solution to the optimization problem

$$\underset{\boldsymbol{w}}{\text{minimize}} \quad \boldsymbol{w}^{\mathrm{H}}\boldsymbol{R}\boldsymbol{w} \qquad \text{subject to:} \quad \boldsymbol{w}^{\mathrm{H}}\boldsymbol{a} = 1. \tag{2}$$

Here, the optimal weights are obtained in closed form as [3] $\boldsymbol{w} = (\boldsymbol{a}^{\mathrm{H}}\boldsymbol{R}^{-1}\boldsymbol{a})^{-1}\boldsymbol{R}^{-1}\boldsymbol{a}$. Note that the constraint in (2) forces the beam pattern to have the main beam towards θ_0 with a gain 1. When the estimation of θ_0 has some uncertainty, and we wish to have nulls towards the RFI angles, we can add more constrains, leading to an optimization problem

$$\underset{\boldsymbol{w}}{\text{minimize}} \quad \boldsymbol{w}^{\mathrm{H}}\boldsymbol{R}\boldsymbol{w} \qquad \text{subject to:} \quad \boldsymbol{C}^{\mathrm{H}}\boldsymbol{w} = \boldsymbol{u}. \tag{3}$$

Here, $\boldsymbol{C} \in \mathbb{C}^{N\times L}$ and $u \in \mathbb{C}^L$ define L constrains of which one is the constraint in (2). The optimal weights in closed form are [4] $\boldsymbol{w} = \boldsymbol{R}^{-1}\boldsymbol{C}(\boldsymbol{C}^{\mathrm{H}}\boldsymbol{R}^{-1}\boldsymbol{C})^{-1}\boldsymbol{u}$. See [5] for a detailed description.

III. Radio Interface and Digital System

A. System Overview

A 5.7 GHz RF system with 32-element ULA and receivers with a digital processing back-end on field programmable gate array (FPGA) was implemented to experimental on MVDR and Howells-Applebaum arrays. The setup integrates key subsystems, such as, patch antenna array, RF receiver chains, and FPGA based digital hardware.

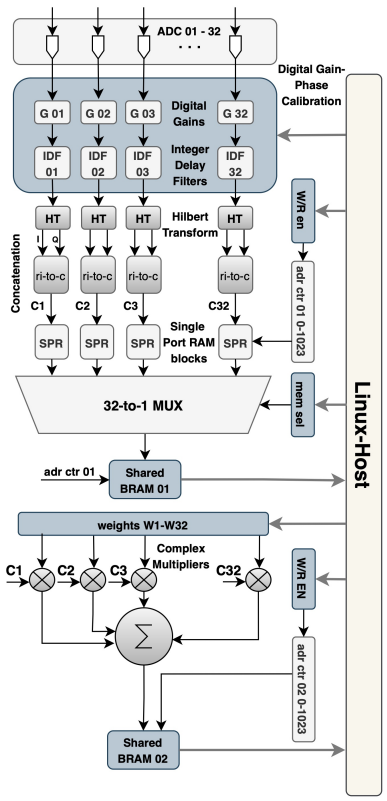

Fig. 1. Digital architecture for 32-channel receiver with Howells-Applebaum adaptive beamforming. The FPGA processing occurs on a Virtex-6 Sx-475 device installed on a ROACH-2 platform with CASPER open source blocks for standard functions such as ethernet and BRAM access.

Digital compute was incorporated into the FPGA to allow for real-time data manipulation of 32 ADC channels. The system employs the ROACH-2 digital signal processing (DSP) platform which plays a critical role by acting as an interface between the FPGA and the main host system, and a Linux server. This connection is facilitated via a 1 Gbps Ethernet link, enabling seamless communication between the FPGA's memory and the server. A Python routine running on the Linux server controls operations and retrieves data from the FPGA memory while iteratively scanning through various angles. The modular and re-configurable design of the system enhances both flexibility and scalability, making it a versatile platform for a wide range of advanced signal processing experiments.

B. Antennas, Electronics, ADC, and FPGA

The RF front end of the receiver is built with a 32-element uniform linear array (ULA) at $5.7\,\mathrm{GHz}$, connected to 32 direct-conversion RF receiver chains on PCBs. The array elements are spaced 0.6λ apart, or about $32\,\mathrm{mm}$ at this frequency, with each element formed by a vertical subarray of 4×1 5.7-5.8 GHz patch antennas. This configuration supports passive

beamforming in the vertical direction. Each element is fed into parallel heterodyne receivers using a shared local oscillator (LO) system driven by a low-phase-noise oscillator. The receiver chains include low-noise amplifiers (LNAs) offering $16\,\mathrm{dB}$ gain at $5.8\,\mathrm{GHz}$ and a noise figure of $2.4\,\mathrm{dB}$. Post-amplification, signals are filtered using a $4.7\,\mathrm{GHz}$ to $6\,\mathrm{GHz}$ bandpass filter to remove out-of-band noise, downconverted to low intermediate frequency (IF), and further filtered. These 32 low-IF signals are amplified by $30\,\mathrm{dB}$ and then digitized via two ADC16x250-8 converter cards on the ROACH-2 FPGA platform. The ADCs use 8-bit resolution and sampling up to $250\,\mathrm{Msample/s}$ per channel. This setup ensures accurate signal digitization for subsequent processing.

ROACH-2 with Xilinx Virtex-6 Sx-475 FPGA features an integrated processor for communication and control. It connects high-bandwidth input-output (I/O) via two ZDOK interfaces, compatible with two ADC16x250-8 cards. The ADCs were used to sample downconverted intermediate frequency (IF) signals at 200 MS/s rate. A VALON 5015 synthesizer provided the LO and a NOISE XT low-jitter clock synthesizer generated clock signals for the FPGA and ADC. The ADC16x250-8 cards can be accessed and calibrated using CASPER routines.

IV. Adaptive Null Array Processor

The ADCs output 200M signed 8-bit samples per a second with 7 bits assigned for fractional part. Gain and phase calibrated signal values are fed to FIR Hilbert transform blocks. The Hilbert transform block generates in-phase and quadrature signals. A total of 1024 complex samples are written into 1024 distinct memory addresses across 32 single-port RAM blocks. The initiation of writing to the single-port RAM can be triggered at a specific time by writing to a software register through the PPC (PowerPC) link of the ROACH-2 platform. The software registers serve as a common interface accessible by both the FPGA hardware and the ROACH-2 control logic. These registers can be read from or written to using a host computer via the 1 Gbps PPC Ethernet link. After a set of 1024 samples across the 32 elements is written into the single-port RAM blocks, the data from each RAM block is multiplexed to 1024 distinct addresses of a shared BRAM block. This shared BRAM serves as an accessible memory resource, interfacing both the ROACH-2 control logic and the FPGA logic.

Receiver beamformer utilizes element-wise complex samples that are multiplied with complex weight values. These weights are in signed fixed point 16_14 format thus enabling the Linux host to write the weight values to the software registers which holds them without scaling. Our design uses 1024 samples of the beamformed signal which are obtained after the complex adder in the chain are written into 1024 addresses of the shared BRAM 02 as depicted in Fig. 1.

A. Calibration and Snapshot Capture

RF receiver chains are first calibrated. The objective of the digital calibration is to align the 32 sampled signal streams, ensuring uniformity when the antenna array detects the same wavefront across all 32 elements. A double-ridge guided horn antenna was positioned at a distance of 20 meters, directly at the broadside angle, to ensure that the receiver antenna array receives the same planar wave across all elements. During transmission, each of the digital streams is scaled by a gain factor, ranging from 0 to 255, to normalize the amplitude of the received signals. Following the gain calibration, digital phase calibration employs integer delay filters to synchronize the phases of the 32 streams. These filters are capable of introducing delays of 0 to 32 clock cycles per stream, ensuring phase alignment across all elements in the array.

B. Optimum Weight Vector

The snapshot measurements required to learn the nulls of the receiving beam pattern are acquired using the shared BRAM 01 as depicted in Fig. 1. After capturing a set of 1024 samples from the 32 streams, the covariance matrices are read from the Linux host using a Python routine through the PPC link. The captured samples, represented as 32-bit complex words, are then requantized to signed 16_7 fixed-point format for both the real and imaginary components within the Python routine. These fixed-point values are subsequently combined to generate a 32×1024 complex matrix.

A total of 1024 covariance matrices, each of size 32×32, are computed using the columns of a 32×1024 complex matrix. For each column, a corresponding 32×32 covariance matrix is created, and these matrices are averaged to obtain a final covariance estimate. The inverse of this estimate covariance matrix is calculated using an inbuilt *numpy* function and the optimum weight vector is obtained by the dot product between this inverted matrix and the steering vector. The values of the complex optimum weight vector is converted to 32-bit words and written to 32 software registers in the ROACH-2.

V. Experimental Results

The calibration of the system is done in two phases. Once a design is programmed on to the FPGA, the ADCs are enabled & calibrated using Ruby routines provided by the CASPER community [6]. Following ADC calibration, the ADC output streams are digitally fine-calibrated. Two double-ridge guided horn antennas and a sub-array of 4×1 patch antennas were employed to transmit the jamming signals [Fig. 2]. The samples required to learn the nulls were captured by transmitting a 5.71 GHz sinusoidal signal from each antenna with 15 dBm power kept in distinct bearings in 20m distance. Local oscillator f_{LO} was set to 5.7 GHz, resulting in an intermediate frequency of about 10 MHz, with the down-converted outputs digitized at $f_{CLK} = 200MHz$.

Following snapshot capture of RFI, the optimum weight vector is calculated using Howells-Applebaum method in the Linux host and the weight values are written to the weight software registers on the ROACH-2. Power patterns were obtained by transmitting a continuous-wave (CW) signal using a double-ridge guided horn antenna at the broadside 0° angle at a distance of 20m from the receiver array on an open parking deck as depicted in Fig. 2.

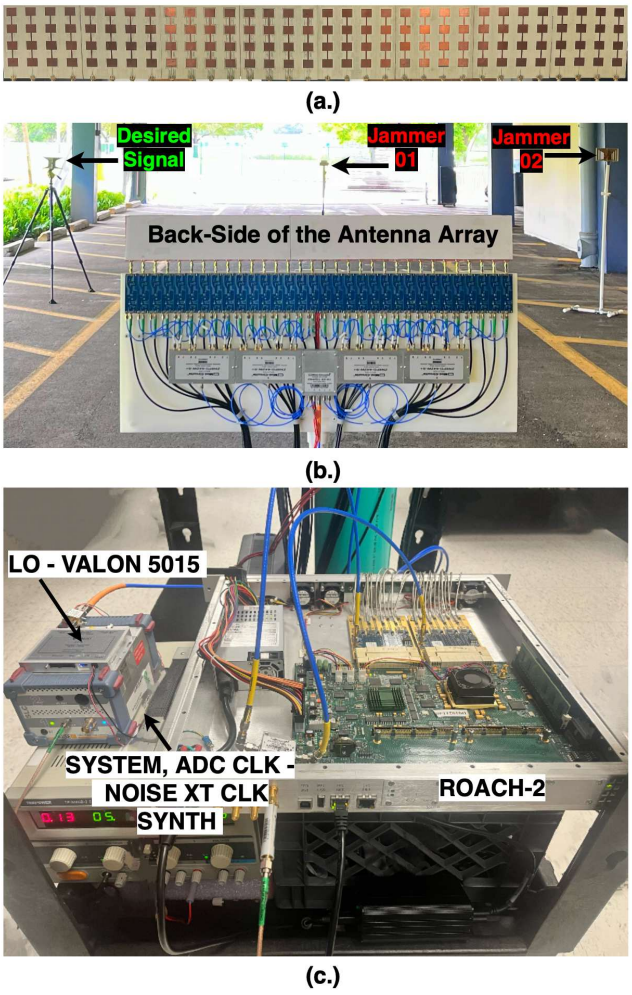

Fig. 2. (a.) Front of the array (b) Overall setup with the antenna placements (c) ROACH-2 FPGA system (Sx-475T FPGA) digital back-end.

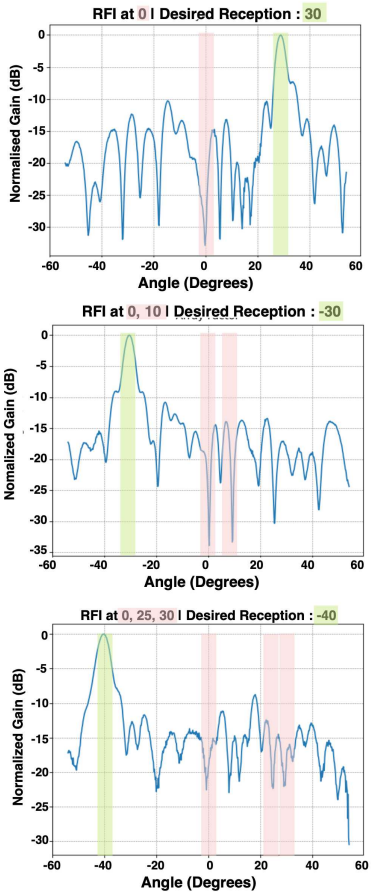

Fig. 3. Measured array patterns for 1, 2 and 3 RFI sources from the real-time 32-channel adaptive aperture. Nulls are nominally 30 dB below main lobe.

Fig. 3 shows measured array factors for three scenarios of RFI placement and desired signal reception. Peaks were observed at the previously set angles in the beam steering vector while maintaining 10 dB directivity against highest side-lobe. Approximately 35 dB depth "nulls" were measured at the angles corresponding to the the RFIs in both 1- and 2-RFI scenarios. In the case of a 3-RFIs, the system maintained more than 20 dB attenuation (the nulls are deeper than that, but difficult to measure in the rotating platform due to the sharp nature of nulls), demonstrating effective interference suppression across multiple sources of RFI.

VI. Conclusions

The ability to null out RFI/jammers using a digital beamformer is quite crucial in many array processors. The proposed fully-digital experimental test-bed has successfully measured RFI, operated on averaging complex-valued covariance matrices across multiple snapshots in real-time, inverted ensemble averaged complex valued covariance matrices on the fly, optimally null-formed using Howells-Applebaum, and operated the optimum beamformer across 32-channel fully-digital FPGA digital receiver array processing at a real-time bandwidth of 100 MHz per beam. The experimentally verified compute architectures and DSP algorithms will be used as a building block for test-bed realization new adaptive radar receivers, spectrum sensors and wireless MIMO radio experiments that must operate with real-time adaptive null-forming for both RFI rich and RF denied(jammed) environments.

References

[1] S. Applebaum, "Adaptive arrays," *IEEE Transactions on Antennas and Propagation*, vol. 24, no. 5, pp. 585–598, Sep. 1976.

[2] P. Howells, "Explorations in fixed and adaptive resolution at GE and SURC," *IEEE Transactions on Antennas and Propagation*, vol. 24, no. 5, pp. 575–584, Sep. 1976.

[3] J. Capon, "High-resolution frequency-wavenumber spectrum analysis," *Proceedings of the IEEE*, vol. 57, no. 8, pp. 1408–1418, Aug. 1969.

[4] N. Jablon, "Adaptive beamforming with the generalized sidelobe canceller in the presence of array imperfections," *IEEE Transactions on Antennas and Propagation*, vol. 34, no. 8, pp. 996–1012, Aug. 1986.

[5] A. M. Elbir, K. V. Mishra, S. A. Vorobyov, and R. W. Heath, "Twenty-five years of advances in beamforming: From convex and nonconvex optimization to learning techniques," *IEEE Signal Processing Magazine*, vol. 40, no. 4, pp. 118–131, Jun. 2023.

[6] A. Madanayake, K. Lawrance, B. U. Kumarasiri, S. Sivasankar, T. Gunaratne, C. U. S. Edussooriya, and R. J. Cintra, "Design of multichannel spectrum intelligence systems using approximate discrete fourier transform algorithm for antenna array-based spectrum perception applications," *Algorithms*, vol. 17, no. 8, 2024. [Online]. Available: https://www.mdpi.com/1999-4893/17/8/338